Photometric Model of a Rain Drop

Kshitiz Garg and Shree K. Nayar
Computer Science Department, Columbia University
500 West 120th Street, Room 450, New York, NY 10027
E-mail: {kshitiz, nayar}@cs.columbia.edu

Abstract

The visual appearance of rain is highly complex. Unlike the particles that cause other weather conditions such as haze and fog, rain drops are large and visible to the naked eye. Each drop refracts and reflects both scene radiance and environmental illumination towards an observer. As a result, a spatially distributed ensemble of drops moving at high velocities (rain) produces complex spatial and temporal intensity fluctuations in images and videos. To analyze the effects of rain, it is essential to understand the visual appearance of a single rain drop.

In this paper, we develop geometric and photometric models for the refraction through, and reflection (both specular and internal) from, a rain drop. Our geometric and photometric models show that each rain drop behaves like a wide-angle lens that redirects light from a large field of view towards the observer. From this, we observe that in spite of being a transparent object, the brightness of the drop does not depend strongly on the brightness of the background. Our models provide the fundamental tools to analyze the complex effects of rain. Thus, we believe our work has implications for vision in bad weather as well as for efficient rendering of rain in computer graphics.

Keywords: Rain drops, Photometric model, Radiance, Refraction, Reflection, Panorama, Perspective view, Dispersion.

Photometric Model of a Rain Drop

Please view images in color.

Abstract

The visual appearance of rain is highly complex. Unlike the particles that cause other weather conditions such as haze and fog, rain drops are large and visible to the naked eye. Each drop refracts and reflects both scene radiance and environmental illumination towards an observer. As a result, a spatially distributed ensemble of drops moving at high velocities (rain) produces complex spatial and temporal intensity fluctuations in images and videos. To analyze the effects of rain, it is essential to understand the visual appearance of a single rain drop.

In this paper, we develop geometric and photometric models for the refraction through, and reflection (both specular and internal) from, a rain drop. Our geometric and photometric models show that each rain drop behaves like a wide-angle lens that redirects light from a large field of view towards the observer. From this, we observe that in spite of being a transparent object, the brightness of the drop does not depend strongly on the brightness of the background. Our models provide the fundamental tools to analyze the complex effects of rain. Thus, we believe our work has implications for vision in bad weather as well as for efficient rendering of rain in computer graphics.

Photometric Model of a Rain Drop

Abstract

The visual appearance of rain is highly complex. Unlike the particles that cause other weather conditions such as haze and fog, rain drops are large and visible to the naked eye. Each drop refracts and reflects both scene radiance and environmental illumination towards an observer. As a result, a spatially distributed ensemble of drops moving at high velocities (rain) produces complex spatial and temporal intensity fluctuations in images and videos. To analyze the effects of rain, it is essential to understand the visual appearance of a single rain drop.

In this paper, we develop geometric and photometric models for the refraction through, and reflection (both specular and internal) from, a rain drop. Our geometric and photometric models show that each rain drop behaves like a wide-angle lens that redirects light from a large field of view towards the observer. From this, we observe that in spite of being a transparent object, the brightness of the drop does not depend strongly on the brightness of the background. Our models provide the fundamental tools to analyze the complex effects of rain. Thus, we believe our work has implications for vision in bad weather as well as for efficient rendering of rain in computer graphics.

1 Vision and Rain

Weather can greatly impair the performance of outdoor vision systems. Outdoor vision systems are used in various applications, such as surveillance, autonomous navigation and remote sensing. Today, none of these systems account for the effects of weather conditions. To enable outdoor systems to perform in all weather conditions we need to model and remove the effects of weather.

The visual effects produced by different weather conditions can be classified into two main categories: steady (fog, mist and haze) and dynamic (rain, hail and snow). In steady weather, the individual water droplets that constitute the weather are too small ($1 - 10\,\mu$m) to be individually detected by a camera. The intensity at a pixel in steady weather is due to the aggregate effect of a large number of these drops within the pixel's solid angle. Hence, simple models of atmospheric scattering, such as attenuation and airlight [8], can be used to adequately describe the effects of steady weather. Recently, the visual manifestations of steady weather have been modeled and used for en-

<table>
<tr><td>(a)</td><td>(b)</td></tr>
</table>

Figure 1: The visual appearance of rain. (a) Streaks of rain due to the motion of individual rain drops. (b) A zoomed-in image of a water drop. Note the complex intensity pattern produced by the drop. Such patterns arise due to the intricate optical properties of rain drops. A model for the appearance of a drop is critical to understanding the visual manifestations of rain.

hancing the quality of images taken in poor weather [9, 10].

On the other hand, dynamic weather conditions, such as rain and snow, produce much more complex visual effects. Rain drops are large enough ($1 - 10\,$mm) to be individually detected by the camera. Furthermore, their motions produce randomly varying spatial and temporal intensities in an image. Figure 1(a) shows streaks in an image due to motion blur of individual rain drops. Figure 1(b) shows a zoomed in image of a water drop. Note that a single rain drop can be viewed as an optical lens that refracts and reflects light from the environment towards an observer, as shown by the complex intensity pattern within the drop in Figure 1(b).

Rain has been studied extensively in atmospheric sciences and remote sensing [7, 11, 2]. These studies primarily use active illumination sources (such as lasers) and specialized detectors (such as photo-cells) to examine the effects of rain on a transmitted signal. However, the effects of rain on a passive camera viewing a scene in a natural environment are very different from the effects analyzed in the above studies.

This paper explores the visual appearance of a single rain drop in an image. Since the complex intensity patterns produced by rain in an image (see Figure 1(a)) are due to individual drops, we believe that modeling the appearance of a drop is fundamental to analyzing effects of rain on an imaging system. We begin by describing

1

the physical properties of rain drops, such as their shape, size and velocity distributions. Then, we develop photometric models for the refraction through, as well as the specular and internal reflections from, a rain drop. We extensively verify these models using experiments with actual drops as well as acrylic spheres.

Our geometric and photometric models show that each rain drop behaves like a wide-angle lens that redirects light from a large field of view towards the observer. From this, we observe that in spite of being a transparent object, the brightness of the drop does not depend strongly on the brightness of the background. This observation can have implications for detecting and removing rain from images and videos. Our analytic models can also be used in computer graphics to efficiently render natural phenomena that involve a large number of drops such as rain and water falls. To our knowledge, this is the first work that provides a thorough analysis of the visual effects produced by a rain drop on an imaging system.

2 Physical Properties of Rain Drops

Rain drops differ widely in their shapes, sizes and velocities. In this section, we describe widely used empirical models for the shapes, sizes and velocities of rain drops, which we will use later in deriving our appearance models.

2.1 Shape of a Rain Drop

Smaller rain drops are generally spherical in shape. However, as the size of the drop increases, it becomes an oblate spheroid. Beard and Chuang [1] describe the shape of a rain drop as a 10th order cosine distortion of a sphere :

$$r(\theta) = a\left(1 + \sum_{n=1}^{10} c_n cos(n\theta)\right), \qquad (1)$$

where, a is the radius of the undistorted sphere, $c_1 \ldots c_{10}$ are the coefficients that depend on the radius of the drop and θ is the polar angle of elevation. $\theta = 0$ corresponds to the direction of the fall. The shapes of the drops of various sizes $(0.5 - 2.5 \, \text{mm})$ are shown in Figure 2(a).

2.2 Size of a Rain Drop

Rain drops have a wide size distribution. A commonly used empirical distribution for rain drop size is the Marshall-Palmer distribution [6]:

$$N(a) = 8 \times 10^6 e^{-8200*h^{-0.21}a} \ , \qquad (2)$$

where, h is the rain rate given in mm/hr, a is the radius of the drop in meters and $N(a)$ is the number of rain drops per unit volume that contains sizes within the interval $(a, a+da)$. Figure 2(b) shows the Marshall-Palmer
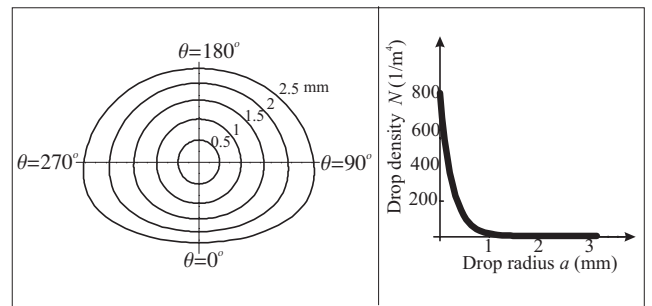
(a) Shapes of rain drops   (b) Drop Size distribution

Figure 2: (a) The shapes of rain drops of various sizes $(0.5 - 2.5 \, \text{mm})$. The bases of the drops are flattened in the direction of fall ($\theta = 0$), mainly due to air pressure. Large drops are severely distorted, while smaller drops are almost spherical. (b) Marshall-Palmer drop size distribution: The number density of a rain drop as a function of drop size (for rainfall rate of 30mm/hr). Note that density of drops decreases exponentially with drop size.

distribution for a typical rainfall rate of 30 mm/hr. Note that the drops that make up a significant fraction of rain are less than 1 mm in size. As seen from Figure 2(a), the drops with radii less than 1 mm are not severely distorted and their shapes can be well approximated by a sphere. Therefore, in this paper, we will model rain drops as transparent spheres of water.

2.3 Velocity of a Rain drop

As a rain drop falls, it attains a constant velocity, called the terminal velocity [5]. Gunn and Kinzer [3] present an empirical study of the terminal velocities of falling rain drops for different drop sizes. Their observations show that the terminal velocity of a rain drop can be expressed as a function of its size and is given by

$$v = 9.40\left(1 - e^{-3.45\,10^3 a^{1.31}}\right), \qquad (3)$$

where, v is in (meters/sec) and a is in meters.

3 Appearance of a Rain Drop

The appearance of a rain drop is determined by the environmental illumination it refracts and reflects (both specular and internal reflections) towards the observer. In this section, we develop the geometric and photometric models of refraction through, and reflections (specular and internal) from, a rain drop.

Figure 3 shows the geometry of refraction through and reflection from the drop. Ray $\hat{r}$ reaches the camera after being refracted through the drop. Ray $\hat{s}$ reaches the camera after specular reflection from the drop and ray $\hat{p}$ after being internally reflected by the drop. The refracted, specularly reflected and internally reflected rays emerge from the same point B on the drop. Hence, the

radiance L of point B in the direction of the camera is the sum of the radiances L_r, L_s and L_p due to refraction, specular and internal reflection, respectively:

$$L(\hat{n}, \hat{v}) = L_r(\hat{n}, \hat{v}) + L_s(\hat{n}, \hat{v}) + L_p(\hat{n}, \hat{v}). \qquad (4)$$

Here, $\hat{n}$ is the surface normal at B and $\hat{v}$ is the viewing direction of the camera. We drop $\hat{v}$ from the above expression since it can be parameterized in terms of $\hat{n}$, and write

$$L(\hat{n}) = L_r(\hat{n}) + L_s(\hat{n}) + L_p(\hat{n}). \qquad (5)$$

The radiances L_r, L_s and L_p are determined from the environmental radiance L_e. Thus, we rewrite equation (5) as

$$L(\hat{n}) = R\, L_e(\hat{r}) + S\, L_e(\hat{s}) + P\, L_e(\hat{p}), \qquad (6)$$

where, R, S and P are defined as the *radiance transfer functions* for refraction, reflection and internal reflection. In the following sections we derive exact expressions for these transfer functions and the geometric mapping from ray directions $\hat{r}$, $\hat{s}$ and $\hat{p}$ to the normal $\hat{n}$.

To derive the geometric mapping, we define a local coordinate frame placed at the center of the drop with its z-axis aligned with the optical axis of the camera. Note that we have made this choice only to simplify the derivation of the mapping. When the drop lies elsewhere, the z-axis of the local coordinate frame can be aligned with the viewing direction that passes through the center of the drop[1].

Since the drop size is very small compared to its distance from the camera and the environment, all ray directions are defined with respect to the center of the drop coordinate frame. In our analysis, we use either vector or angle notations. That is, a direction $\hat{a}$ may also be denoted as (θ_a, ϕ_a), where θ_a is the polar angle and ϕ_a is the azimuthal angle. The image coordinates of the drop are parameterized as (ρ, ϕ), where ρ is the distance of an image point from the center of the circular image of the drop (see Figure 3). The coordinates (ρ, ϕ) are related to $\hat{n} \equiv (\theta_n, \phi_n)$ as

$$\rho = m\, a\, sin\, \theta_n, \quad \phi = \phi_n. \qquad (7)$$

Here, $m = \frac{f}{z}$ is the magnification of the camera, f is the effective focal length of the camera and z is the distance of the drop from the camera.

3.1   Contribution of Refraction

We now model the appearance of a rain drop solely due to refraction. In Figure 3, the scene ray $\hat{r} \equiv (\theta_r, \phi_r)$ that
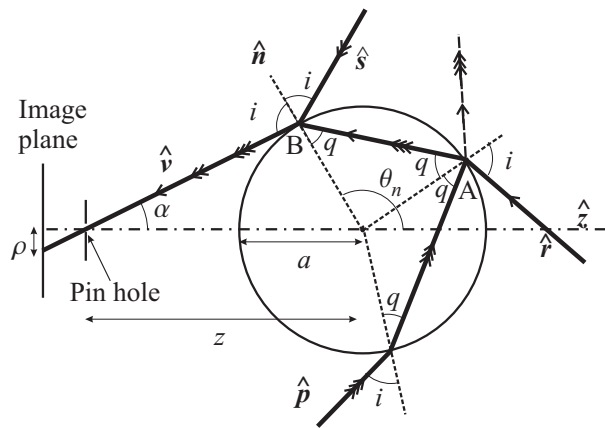
Figure 3: Refraction, specular reflection and internal reflection by a rain drop. Light rays from directions $\hat{r}$, $\hat{s}$ and $\hat{p}$ reach the camera via refraction, specular reflection and internal reflection from the drop, respectively. Therefore, a drop's appearance is a complex mapping of the environmental radiance.

emerges from point B after refraction is related to the normal $\hat{n} \equiv (\theta_n, \phi_n)$ at B by Snell's Law and the shape of the drop. This relation is derived in Appendix I and is found to be:

$$
\begin{aligned}
\theta_r &= 2(\pi - \theta_n) + \alpha + 2sin^{-1}\left(\frac{sin(\theta_n + \alpha)}{\mu}\right), \\
\phi_r &= \pi + \phi_n.
\end{aligned}
\qquad (8)
$$

Here, α is the angle between the ray $\hat{v}$ and the optical axis of the camera.

We now derive the radiance transfer function R that relates the drop radiance $L_r(\hat{n})$ to the environmental radiance $L_e(\hat{r})$. The radiance of ray $\hat{r}$ only changes at the interface points A and B. The radiance L_A of the refracted ray at interface point A is derived in Appendix II and is given by

$$L_A = ((1 - k(i, \mu))\, \mu^2 L_e(\hat{r}), \qquad (9)$$

where, i is the incident angle, μ is the refractive index of the water and k is the Fresnel's reflectivity coefficient for unpolarized light[2]. Similarly, the radiance $L_r(\hat{n})$ at point B with surface normal $\hat{n}$ is given by

$$L_r(\hat{n}) = \left(1 - k\left(q, \frac{1}{\mu}\right)\right)\left(\frac{1}{\mu}\right)^2 L_A. \qquad (10)$$

Here, q is the angle the refracted ray makes with the surface normal at B. Substituting L_A from equation (9)

and noting that $k(q, \frac{1}{\mu}) = k(i, \mu)$ we obtain the radiance due to refraction as

$$L_r(\hat{n}) = (1 - k(i, \mu))^2 L_e(\hat{r}). \qquad (11)$$

Hence, the radiance transfer function R is given by

$$R = (1 - k(i, \mu))^2, \qquad i = \pi - \theta_n - \alpha. \qquad (12)$$

3.2 Contribution of Reflection

The direction $\hat{s} \equiv (\theta_s, \phi_s)$ of specular reflection is related to the surface normal $\hat{n} \equiv (\theta_n, \phi_n)$ as

$$
\begin{aligned}
\theta_s &= 2\theta_n - \pi - \alpha, \\
\phi_s &= \phi_n.
\end{aligned} \qquad (13)
$$

The radiance of the specular ray $\hat{s}$ changes only at point B and is given by

$$L_s(\hat{n}) = k(i, \mu) L_e(\hat{s}), \qquad (14)$$

where, k is the Fresnel's reflectivity coefficient. Hence, the radiance transfer function for reflection is simply

$$S = k(i, \mu), \qquad i = \pi - \theta_n. \qquad (15)$$

3.3 Contribution of Internal Reflection

We now model the appearance of a drop due to one or more internal reflections from the inner surface of the drop. Figure 3 shows a scene ray $\hat{p} \equiv (\theta_p, \phi_p)$ reaching the observer after an internal reflection[3] from point A. The direction of $\hat{p}$ is related to the surface normal $\hat{n} \equiv (\theta_n, \phi_n)$ at point B. In Appendix I, we derive the geometric mapping from θ_p to θ_n for a ray that reflects N times from the inner surface of the drop before exiting the drop:

$$
\begin{aligned}
\theta_p &= 2(i - q) + N(\pi - 2q) - \alpha, \\
\phi_p &= \phi_n,
\end{aligned} \qquad (16)
$$

where, $i = \pi - \theta_n$ and $q = sin^{-1}(\frac{sin\, i}{\mu})$.

In this case, the radiance $L_p(\hat{n})$ of the ray $\hat{p}$ changes N times due to reflection and twice due to refraction. From equations (11) and (14), we obtain

$$L_p(\hat{n}) = k(i, \mu)^N (1 - k(i, \mu))^2 L_e(\hat{p}). \qquad (17)$$

Hence, the radiance transfer function for internal reflection is

$$P = k(i, \mu)^N (1 - k(i, \mu))^2, \qquad i = \pi - \theta_n. \qquad (18)$$

Since $k < 1$, P decreases for increasing N and can be neglected [4] for $N > 2$.

---

[3]Note that this is a partial internal reflection. It is easy to show from the geometry of a sphere that total internal reflections can never occur in a spherical drop since the maximum angle q_{max} that a ray inside the drop can make with the surface normal is always less than the critical angle of internal reflection.
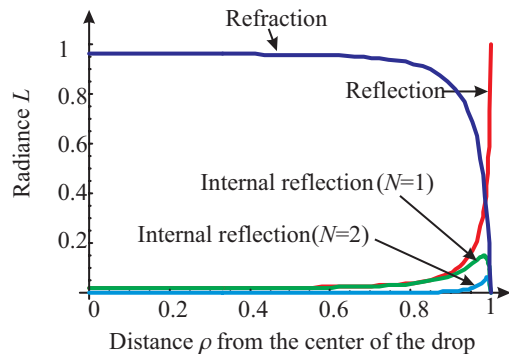

Figure 4: Drop radiance due to reflection, refraction and internal reflection plotted as a function of the distance ρ (see equation (7) and Figure 3). Here, $L_e = 1$. The radiance of the drop is mainly due to refraction. Specular and internal reflections are significant only at the periphery of the drop.

3.4 Composite Appearance of a Rain Drop

The composite appearance of a rain drop is given by the sum of the radiances due to specular reflection, refraction and internal reflections (see equation (6)). Substituting R, S and P from equations (12), (15) and (18), into equation (6), we get

$$
\begin{aligned}
L(\hat{n}) &= (1 - k(i, \mu))^2 L_e(\hat{r}) + k(i, \mu) L_e(\hat{s}) \\
&\quad + \sum_{N=1}^{2} k(i, \mu)^N (1 - k(i, \mu))^2 L_e(\hat{p}). \quad (19)
\end{aligned}
$$

Figure 4 shows the radiance of a surface point due to reflection, refraction and internal reflection ($N = 1$ and $N = 2$) as a function of distance ρ (see equation (7) and Figure 3). For illustration purposes, we assume orthographic projection ($\alpha = 0$) and uniform environmental radiance of ($L_e = 1$). It is seen that the radiance of the drop is mainly due to the refraction, except at the periphery of the drop where the radiances due to reflection and internal reflections are significant.

Specular and internal reflections can also be significant when the environment consists of bright light sources. For example, on a sunny day the specular reflection of sunlight from the drop's surface significantly contributes to the brightness of the drop. In addition, internal reflections can disperse sunlight into its constituent colors, to form a rainbow. Note that since the refractive index depends on the wavelength of light, our appearance model can easily reproduce the visual effects produced by the dispersion of light from rain drops. In summary, we have developed a comprehensive model for the appearance of a rain drop.
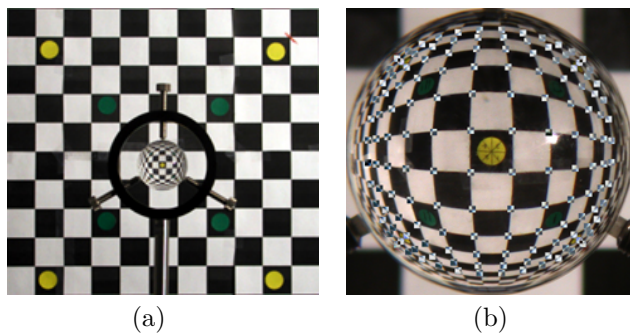
4

(a)   (b)

Figure 5: (a) Experimental setup to verify the geometric mapping due to refraction. An acrylic ball of radius 0.875 inches is placed in front of the checkerboard pattern. (b) The locations of the corners in the checkerboard pattern are used to compute their locations in the image using the geometric mapping model(8). The computed locations are overlaid on the captured image. The RMS error in the mapping was found to be 3.5 pixels which is 1% of the diameter of the sphere (in pixels).

4   Experimental Verification

In this section, we conduct experiments to verify the geometric and photometric models derived in the previous section.

Verification of Geometric Mapping: We have conducted experiments to verify the accuracy of the refraction mapping given by equation (8). Figure 5(a) shows the experimental setup. An acrylic ball ($\mu = 1.49$) of radius 0.875 inches was placed 85 inches from the camera. The checkerboard pattern was placed 6 inches from the center of the acrylic ball. The pixel coordinates of the corners of the checkerboard pattern were calculated using equation (8) and were compared with the actual corner locations measured in the image. In figure 5(b), the locations of the corners computed using the model are overlaid on the captured image. The percentage RMS error in the mapping is found to be 3.5 pixels which is less than 1% of the diameter of the sphere (in pixels). The small error in the result is mainly due to the assumptions of orthographic projection and distant background. Nevertheless, the result verifies the accuracy of our model.

Verification of Drop Photometry: Figure 6(a) shows the experimental setup used to verify the photometric model of refraction[4]. The acrylic ball of radius 0.875 inches was placed 9 inches from a calibrated light box. Figure 6(b) shows the actual image obtained from a camera with a linear radiometric response. Figure 6(c) shows the image computed using the photometric model in

---

[4]Since the light source is placed behind the acrylic ball, specular and internal reflections are insignificant (except at edges) and have been ignored.

(a)

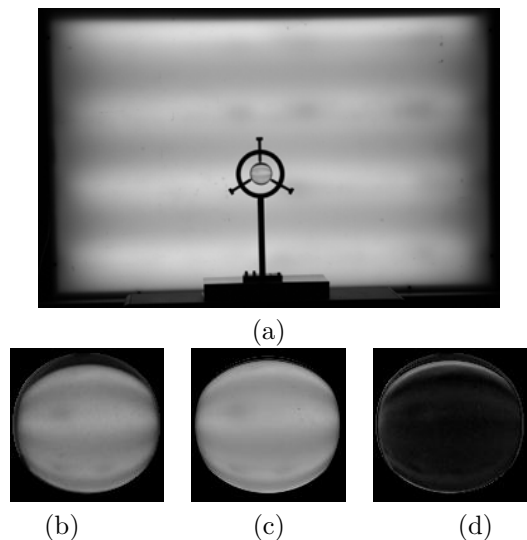(b)   (c)   (d)

Figure 6: Verification of the photometry of refraction through a drop. (a) An acrylic ball of radius 0.875 is placed in front of a calibrated light box. (b) The image of the acrylic ball. (c) The image computed using the photometric model in equation (11). (d) An image showing the differences (in gray levels) between the actual image (b) and the predicted image (c). The RMS error is 3 gray levels (out of 256).

equation (11). Figure 6(d) shows the absolute values of the differences in the gray levels of the predicted and the calculated values. The RMS error is 3 gray levels (out of 256). The error at the upper edge of the acrylic ball in figure 6(d) is due to misalignment of camera's optical axis with the horizontal direction. Except in this upper region, the intensity difference is almost zero across the image. This verifies the accuracy of our photometric model.

5   Average Brightness of a Drop

Although rain drops are transparent, their average intensities do not depend strongly on the background scene. This is because drops have large fields of view (almost an entire hemisphere) and typically the background scene subtends only a small angle at the drop. To verify this, we captured a video of drops falling against a known background under an overcast sky. The background (see Figure 7(a)) is a plane with horizontal stripes of different shades of gray and was placed 3 meters from the falling drops. Six different drop-sized regions (marked A through F) in the image (corresponding to different background shades) were monitored over time as the drops passed through them. The aggregate brightness of each of these regions is plotted in Figure 7(b) as a function of time. Each spike in the plots corresponds to the sudden change in the brightness of a region as a drop passes through it. It is important to note that all of these spikes
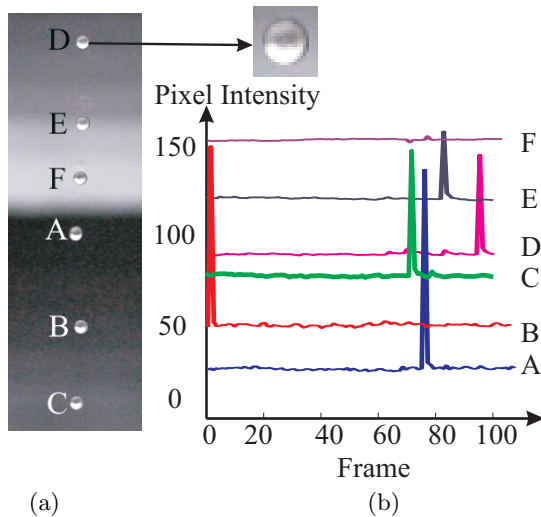
(a)   (b)

Figure 7: Brightness levels produced by rain drops. (a) Setup for the experiment. The background consists of a plane with six horizontal stripes of different shades of gray and is placed 3 meters from the falling drops. (b) The average brightness produced by a drop-sized region on each of the six stripes (marked A through F), plotted as a function of time. The spikes correspond to the sudden increases in brightness when drops pass through the measured regions.

(irrespective of the background brightness) are positive and comparable in magnitude. This result shows that rain drops are typically brighter than their backgrounds and their brightnesses do not depend strongly on the background. This observation can have implications for detecting and removing rain from images and videos.

6 Rendering a Rain Drop

In this section, we show how to render the appearance of a rain drop using our geometric and photometric models. The environment map around the drop is represented as a spherical panorama. For each ray that enters the camera, we find the corresponding scene points in the environment that refract and reflect (both specular and internal) through the rain drop. For this, we use the geometric mapping equations derived in Section 3. To find the brightness of a pixel corresponding to a ray that enters the camera, we use the radiance transfer functions of refraction and reflection derived in Section 3.

Figure 8 illustrates our method for rendering a rain drop. The environment map was obtained using a high resolution omnidirectional imaging system. The spherical panorama of the environment map is shown in Figure 8(a). Figure 8(b) shows the rendered image of a drop with the defocused background scene. Figure 8(c) shows a magnified image of the drop. Notice that the appearance of the drop is dominated by refraction as is evi-

(a) Environmental Illumination

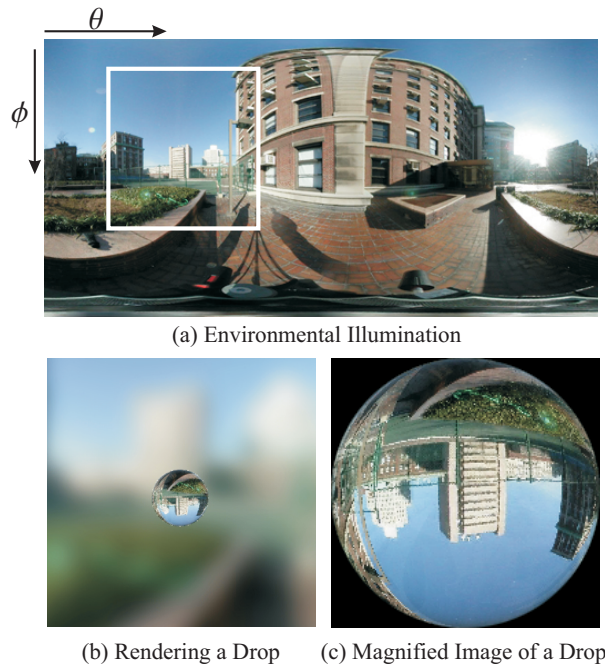(b) Rendering a Drop   (c) Magnified Image of a Drop

Figure 8: Rendering Rain Drops. (a) Spherical panorama obtained from using omnidirectional camera. (b) A drop rendered using the photometric models developed in section 3 (c) A maginified image of the drop. The white box on the spherical panorama (see Figure 8(a)) marks the portion of the environment that is visible through the drop.

denced by the inverted view of the environment. This analytic model can also be used for fast rendering of a variety of natural phenomena that involve a large number of water drops such as rain and water falls.

7 Capturing the World in a Drop

A rain drop refracts light from a wide range of angles into the camera. The field of view of a drop can be obtained using equation (8) by calculating the maximum permissible value of θ_r over all possible angles θ_n (i.e $0 \leq \theta_n \leq 90^o$). It is easy to verify that the **field of view of the rain drop is approximately 165°**. Note that a typical fish-eye lens has a very similar field of view. Therefore, when it rains, each rain drop that is within the depth of field of the imaging system produces wide angle view of the environment. In short, rain results in numerous *natural* omni-directional imaging systems that project the world onto the same image plane, albeit at a very low resolution.

Since we know the geometric mapping of the environment due to a rain drop, we can use it to undo distortions in the wide angle view produced by a drop. This is illustrated in Figure 9. Figure 9(a) shows an image of the falling drop taken with high shutter speed (left) and a magnified image of the drop (right). Using the geomet-
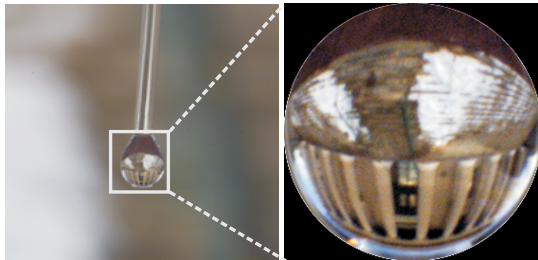
6
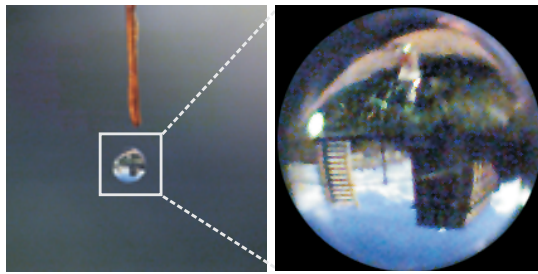
(a) High shutter speed image of a drop.
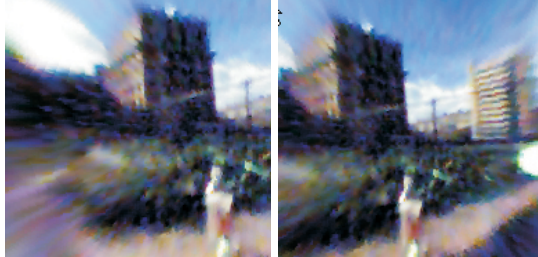
(b) Perspective views created from (a).

(c) An image of a drop hanging from a pipette.

(d) Perspective views created from (c).

Figure 9: Looking at the world through a rain drop. (a) Actual image of a falling drop taken using a high shutter speed, and a magnified image of the drop. (b) Near-perspective views computed using the geometric mapping due to refraction (see equation (8)). (c) An image of a drop hanging from a pipette and a magnified version. (d) Near-perspective views computed using the geometric mapping due to refraction. Note that, in the perspective views, straight lines in the scene are mapped to straight lines in the image.

ric mapping of equation (8), we created near-perspective views of the scene, as shown in Figure 9(b). Figure 9(c) shows an image of a drop hanging from a pipette. The computed near-perspective views are shown in figure 9(d). One may take this notion of the "world in a drop" one step further by observing that two drops in the field of view provide two distinct views of the same scene that can be used to compute the structure of the scene.

8 Conclusion

We developed geometric and photometric models for the appearance of a rain drop due to refraction through the drop as well as reflection from the drop. We showed that a rain drop acts like a wide-angle lens with a field of view of approximately 165°. Our photometric models explain why rain drops do not depend strongly on their backgrounds. This makes it easier to detect and remove rain. We verified these models using experiments with real water drops as well as acrylic spheres.

The models developed in this work are fundamental to analyzing intensity fluctuations produced by rain in images and videos. We believe our models have wide applications in the field of computer vision and graphics. For instance, in computer vision, the model can be used for detection and removal of rain streaks from images and videos. In computer graphics, our analytic models can be used for fast rendering of a variety of natural phenomena that involve a large number of water drops such as rain and waterfalls. Rain streaks (motion blur due to falling drops) can be rendered using the standard motion blur technique in graphics. We are currently exploring the above applications of the model.

References

[1] K.V. Beard and C. Chaung. A new model for the equilibrium shape of raindrops. *Journal of Atmospheric Science*, 44(11):1509–1524, 1987.

[2] S.G. Bradley, C.D. Stow, and C.A. Lynch-Blosse. Measurement of rainfall properties using long optical path imaging. *American Meteorological Society*, 1999.

[3] R. Gunn and G.D. Kinzer. The terminal velocity for water droplet in stagnant air. *Journal of Meterology*, 6:243–248, 1949.

[4] Van De Hulst. *Light Scattering by small Particles*. John Wiley and Sons, 1957.

[5] R.M Manning. *Stochastic Electromagnetic Image Propogation*. McGraw-Hill, Inc, 1993.

[6] J.S Marshall and W.M.K Palmer. The distribution of raindrops with sizes. *Journal of Meterology*, 5:165–166, 1948.

[7] B.J Mason. *Clouds, Rain and RainMaking*. Cambridge University Press, 1975.

[8] E.J. McCartney. *Optics of the Atmosphere: Scattering by molecules and particles.* John Wiley and Sons, 1975.

[9] S.G. Narasimhan and S.K. Nayar. Vision and the atmosphere. *IJCV*, 48(3):233–254, August 2002.

[10] J.P. Oakley and B.L. Satherley. Improving image quality in poor visibility conditions using a physical model for degradation. *IEEE Trans. on Image Processing*, 7, February 1998.

[11] T. Wang and R.S Clifford. Use of rainfall-induced optical scintillations to measure path-averaged rain parameters. *Journal Opt. Soc. America*, 8:927–937, 1975.

Appendix

I: Refraction and Internal Reflection

(a) Refraction: Consider the scene ray $\hat{r}$ in Figure 10). The angle d_r by which the scene ray $\hat{r}$ deflects due to refraction can be calculated by using geometric optics (triangle OAB in Figure 10) and is given by $d_r = 2(i-q)$ The angle θ_r made by the ray $\hat{r}$ with the z-axis (triangle OCP in Figure 10) is given by: $\theta_r = d_r - \alpha$, where, α is the angle between $\hat{v}$ and the optical axis of the camera. Substituting value of d_r, q and $i = (\pi - \theta_n + \alpha)$, in the equation for θ_r we get the result in equation (8).

(b) Internal Reflection: Consider the scene ray $\hat{p}$ in Figure 10). The angle d_p that the scene ray deflects to reach the observer is obtained by adding the angle of deflection $(i - q)$ at point C (refraction), $(\pi - 2q)$ at point A (internal reflection) and $i - q$ at exit point B. Hence, $d_p = 2(i - r) + (\pi - 2q)$. If the scene ray reflects N times from the inside surface of the drop, the angle of deflection is equal to $d_p = 2(i - q) + N(\pi - 2q)$. The angle θ_p that the scene ray $\hat{p}$ makes with the optical axis can be written as $\theta_p = d_p - \alpha$. Substituting value of d_p, in the equation for θ_p, we obtain equation (16).

II Radiance of Refracted Light

In this section, we relate the radiance of the refracted ray to that of the incident ray. Consider a patch of area dA, the flux impinging on this plane from direction $\hat{r}$ (see figure 10),

$$dF_r = L_r \cos i \; d\omega_i \, dA \,, \qquad (20)$$

where, i is the incidence angle, $d\omega_i = \sin(i)di d\phi$ is the solid angle and L_r is the radiance in the direction $\hat{r}$.

Similarly, the flux dF_A in the direction of the ray refracted at point A (see figure 10) is given by

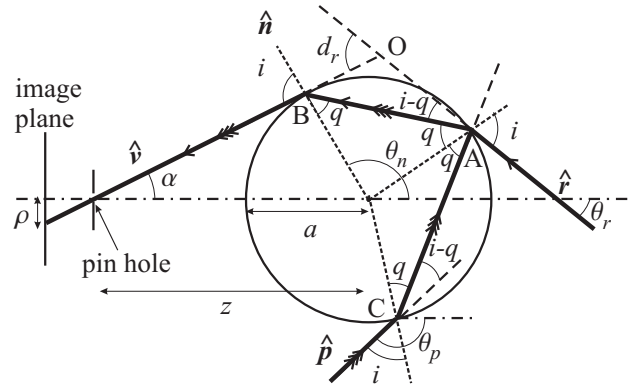$$dF_A = L_A \cos q \; d\omega_q \, dA \,, \qquad (21)$$

Figure 10: Rays of light from directions $\hat{r}$ and $\hat{p}$ are refracted by the drop towards the camera. The geometric mappings of the rays from scene directions $\hat{r}$ and $\hat{p}$ to the surface normal $\hat{n}$ are unique.

where, q is the angle of refraction given by Snell's law and L_A is the of the ray refracted at point A.

The amount of the refracted flux is related to the incident flux via Fresnel's coefficient k and is given by

$$dF_A = (1 - k(i)) \; dF_r \,, \qquad (22)$$

where, $k(i)$ is the Fresnel's reflectivity coefficient for unpolarized light. Substituting the values of dF_A and dF_r in the equation (22) we get

$$L_A = (1 - k(i)) \frac{\cos i}{\cos q} \frac{\sin i \, di}{\sin q \, dr} \, L_r \,. \qquad (23)$$

Using Snell's law to relate di and dr the above equation simplifies to

$$L_A = \mu^2 (1 - k(i)) L_r \,. \qquad (24)$$